Short communication

# Construction of 0D/2D composites heterostructured of CdTe QDs/ZnO hybrid layers to improve environmental remediation by a direct Z-scheme

M. Alegría [a], J. Aliaga [a], P. Jofré [a], L. Ballesteros [b], D. Guzmán [c,g], C. Sotomayor-Torres [d,e], G. González [f,**], E. Benavente [a,g,*]

[a] Departamento de Química, Facultad de Ciencias Naturales, Matemática y Medio Ambiente, Universidad Tecnológica Metropolitana, Santiago, Chile
[b] Instituto de Ciencias Químicas Aplicadas, Inorganic Chemistry and Molecular Material Center, Facultad de Ingeniería, Universidad Autónoma de Chile, El Llano, Subercaseaux, 2801 San Miguel, Santiago, Chile
[c] Centro de Nanotecnología Aplicada, Universidad Mayor, Santiago, Chile
[d] Catalan Institute of Nanoscience and Nanotechnology (ICN2), CSIC and BIST, Campus UAB, 08193, Bellaterra, Barcelona, Spain
[e] Institució Catalana de Recerca i Estudis Avancats (ICREA), 08010 Barcelona, Spain
[f] Departamento de Química, Facultad de Ciencias, Universidad de Chile, Santiago, Chile
[g] Programa Institucional de Fomento a la Investigación, Desarrollo e Innovación (PIDi), Universidad Tecnológica Metropolitana, Santiago, Chile

## ARTICLE INFO

## ABSTRACT

Layered hybrid ZnO (2D) intercalated by myristic acid (MA) with (0D) CdTe quantum dots (QDs) was designed to increase the conversion efficiency of photochemical energy. The results showed that the introduction of CdTe QDs in ZnO(MA) layered with more active sites available enhanced the photocatalytic efficiency. The optimal composite sample ZnO(MA)/CdTe (1:0.02) showed excellent dye removal efficiency under simulated solar light irradiation, above 96% after three cyclic experiments. The correlation coefficients possessed the highest reaction rate. This study offers an efficient research approach and vision to support the development of other photocatalytic systems featuring a direct Z scheme.

## 1. Introduction

Semiconductor-based photocatalytic performance under solar light is believed to be an efficient and ecofriendly system for removing numerous hazardous pollutants from wastewater [1,2]. Many semiconductor materials have been applied as photocatalysts; among them, ZnO has been generally employed due to their stability, non-toxicity, safety, low cost, high activity, and morphologies, such as 0D, 1D, 2D, and hierarchical nanostructures [3]. Compared to nanostructures, nanosheets (2D) are more suitable for creating photocatalysts with well performance as they have an elevated specific surface area, plenty active sites, and fast mass diffusion lengths to increase the efficiency of electron transport [4,5]. However, the single component photocatalysis, it very difficult because of the fast recombination of photogenerated electrons and holes. Because of this, in the last few years, the coupling of semiconductors has received increased interest expected to the ability to integrate several semiconductors into one system. Binary coupling is considered a potential method that could pass the obstacles of single semiconductors and greatly improve the photocatalytic performance in various solar-driven reactions, mainly in pollutant degradation [6,7]. It is well recognized that a mediator-free direct Z-scheme photocatalytic system only including two semiconductor components possesses separation efficiency of electrons and holes on distinct semiconductors as well as great redox ability [8,9]. Compared to bulk materials, zero-dimensional (0D) quantum dots (QDs) have more prospective in photocatalytic applications expected to their quantum confinement effect and sizeable surface to volume ratios [10,11]. CdTe QDs are direct band gap semiconductor (1.5–2.3 eV) nanoparticles with strong visible-light absorption ability, which have been utilized in fluorescent imaging of cells [12], solar cells [13,14], and in the construction of a direct Z-scheme [15,16]. Recently, excellent developments have been achieved mixed with materials such as 0D/2D type composite photocatalysts that have a direct Z scheme mechanism; for example, g-$C_3N_4$ QDs/ZnO nanosheets [17] and $MoS_2$ QDs/$C_3N_4$ nanosheets [18] have been
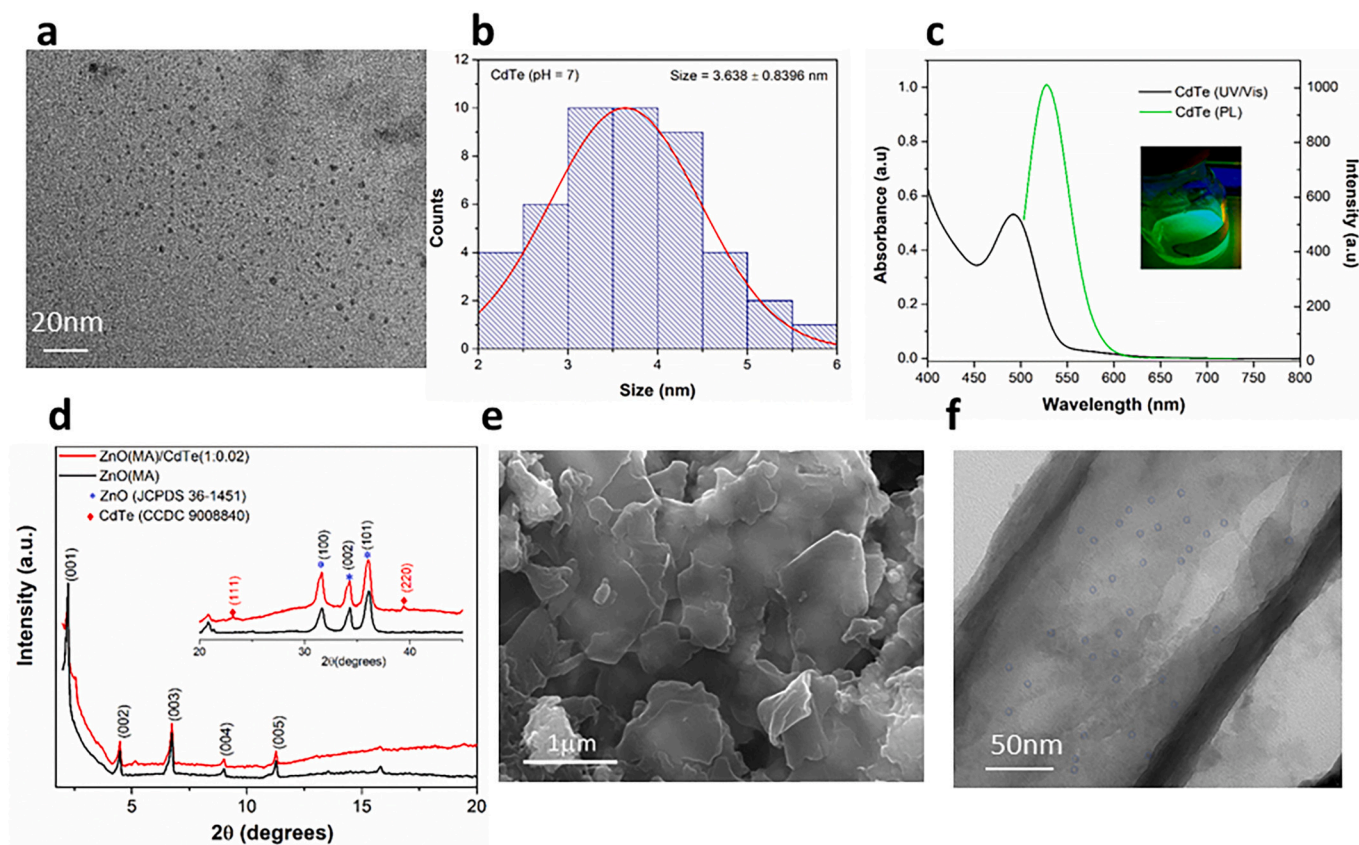
**Fig. 1.** (a) TEM images of CdTe QDs, (b) Size distribution of CdTe QDs, (c) UV–vis absorption and emission spectra of CdTe QDs, (d) XRD patterns of ZnO(MA) and ZnO(MA)/CdTe (e) SEM and (f) TEM images of ZnO(MA)/CdTe.

constructed and utilized in pollutants degradation. They effectively enhance the charge transport capability and photoinduced electron-hole separation efficiency of the composites, thus considerably increasing the photocatalytic performance. Motivated by the reports, an effective approach of coupling CdTe (0D) QDs with ZnO (2D) layered materials was developed for the advancement of additional visible-light-driven photocatalysts for pollution of the environment.

We report a heterostructured nanocomposite formed by a layered hybrid of ZnO combined with CdTe QD nanoparticles. The nano-composite structure consists of ZnO, a self-assembled arrangement of intercalated sheets flanked by myristic acid (MA), which provides properties of a two-dimensional semiconductor, combined with a narrow band semiconductor such as CdTe QD with mercaptosuccinic acid (MSA) as a capping agent, which can expand the absorption range, achieving optimal performance in the degradation of congo red (CR) as a pollutant example under simulated solar light irradiation. The synergy between both semiconductors is corroborated for light absorption and a Z scheme mechanism is proposed to produce the separation of photo-generated electrons and holes and preserve relatively great redox potentials. In addition, the stability and catalytic activity are maintained for three cycles.

## 2. Results and discussion

### 2.1. Characterization of CdTe-QDs

TEM was used to determine the size of the nanocrystals and their distribution (Fig. 1a–b). The average particle size of the synthetized QDs was around $3.64 \pm 0.84$ nm. The UV–vis absorption and emission spectra showed that the absorption peak was at 492 nm and the emission peak was at 528 nm (Fig. 1c). The form of the absorption spectra is

characteristic of quantum dots, and the fluorescence spectrum of the CdTe QDs displays a narrow and clear-cut band representative of the creation of fine crystals [19]. Changes in the absorption and emission spectra towards the red are related to the characteristics of nanocrystals of semiconductor materials and the Stokes changes [20].

### 2.2. Characterization of ZnO(MA)/CdTe-QDs

Fig. 1d shows the XRD patterns of the prepared ZnO(MA) and ZnO (MA)/CdTe nanocomposites. The pattern of ZnO(MA) shows a sequence of Bragg reflections at low 2-theta angles, indicating an ordered layered arrangement. Related interlayer distances, Δd, determined from the positions of the 00 l reflections, of 39.5 Å for ZnO(MA) and ZnO(MA)/ CdTe associate well with the molecular lengths of the myristic acid [21]. In the insert, the pattern shows peaks that may be the hexagonal ZnO wurtzite (JCPDS 36–1451), where the main facets (100), (101) and (002) appeared at $2\theta = 31.7°$, $34.4°$, and $36.5°$, and the CdTe cubic zinc-blend phase shows characteristic peaks corresponding to the (111) and (220) at $2\theta = 23.7°$ and $39.0°$, respectively. The XRD patterns of the nanocomposites exhibit peaks from the CdTe QDs and ZnO(MA), in that way confirming the formation of the required ZnO(MA)/CdTe structure. The reduce diffraction intensity of CdTe could be assigned to the low content of CdTe in the sample. The estimated average crystallite size of material of ~20 nm, as calculated by the Debye Scherer equation, corresponds to nearly 5 single hybrid nanosheets per particle [22]. Fig. 1e shows SEM image of aggregates of lamellar particles produced by assembled nanosheets. EDX elemental mapping of ZnO(MA)/CdTe were completed, clearly indicating that Zn, Cd and Te are distributed in the sample (Fig. SI1). The TEM image of Fig. 1f shows the morphology of the nanosheets/nanoparticles in the ZnO(MA)/CdTe compound. In this figure, the CdTe QD of quite small size, they are highlighted to better
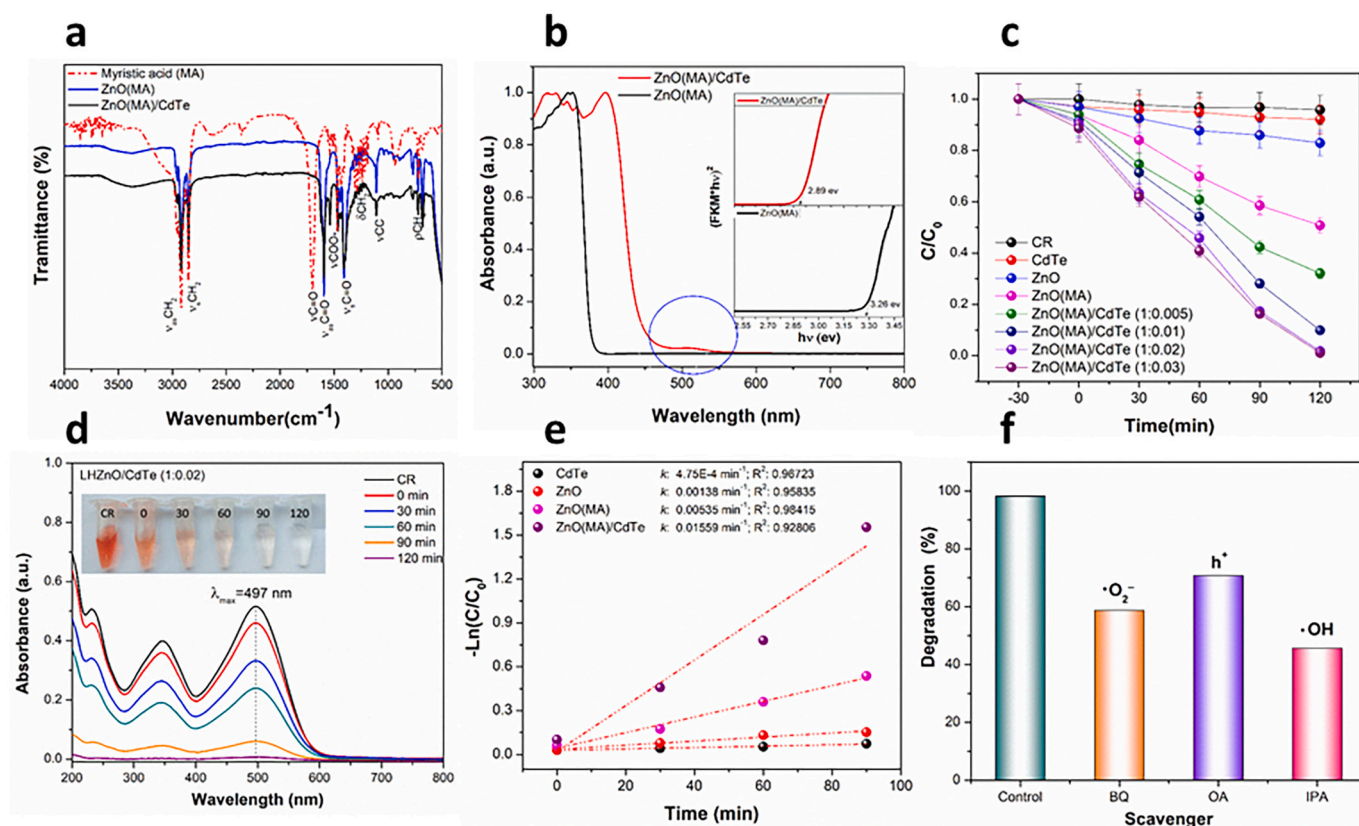
**Fig. 2.** (a) FTIR spectra, (b) UV–Vis spectra, in the insert plots of $(FKM*h\nu)^2$ versus $(h\nu)$ for ZnO(MA) and ZnO(MA)/CdTe, (c) Photocatalytic performance of samples under simulated solar light irradiation (d) UV–vis spectra of the degradation of CR of ZnO(MA)/CdTe (1:0.02) sample, (e) Photodegradation kinetics and (f) Photodegradation of ZnO(MA)/CdTe (1:0.02) for radical scavengers solution.

appreciate their distribution upon the sheets.

Fig. 2a shows the FTIR spectra of MA, ZnO(MA), and ZnO(MA)/CdTe in the range 4000–500 cm$^{-1}$. A comparison of the spectra shows that the main spectral characteristics of myristic acid are present in the nanocomposite and several structural and chemical differences between both compounds are also observed. By contrast of the band at 1700 cm$^{-1}$ related to the $\nu$(C=O) mode of MA, in the ZnO(MA) and ZnO(MA)/CdTe spectrum, we observe the dimeric MA band at 1592 cm$^{-1}$ and 1409 cm$^{-1}$, which corresponds to the modes of vibration $\nu_{as}$(C=O) and $\nu_s$(C=O) of the carboxylate salt, respectively. The values of the separation between the carboxylate stretches among the asymmetric and symmetric stretching modes ($\Delta\nu = 183$ cm$^{-1}$) indicate that the MA is incorporated into ZnO(MA) with a monodentate myristate ligand [23]. The peak at 1500 cm$^{-1}$ observed for the ZnO(MA)/CdTe sample corresponds to the presence of the COO- group of mercaptosuccinic acid. Also, the lack of the −SH peak in the range of 2500–2600 cm$^{-1}$ indicates the formation of the S − Cd bond in the QD. The asymmetric and symmetric CH$_2$ absorptions of the carboxylic acid at 2908 cm$^{-1}$ and 2839 cm$^{-1}$ continue unchanged in the samples.

DRS was utilized to characterize the samples, the absorbed light wavelength dispersal is visibly affected by their electronic bandgap structure, which defines the photocatalytic activity. Fig. 2b shows the UV–vis DRS of ZnO(MA) and ZnO(MA)/CdTe. A sharp fundamental absorbance edge for ZnO(MA) was observed at 378 nm, assigned to the band edge emission or the exciton transition, and a bandgap of 3.26 eV was exhibited. The band gap of the samples was analyzed using the Tauc method. The value of the indirect optical energy gap (Eg), was estimated from a plot of $(\alpha h\nu)^2$ versus the photon energy (h$\nu$) and the intercept of a tangent to the x-axis (in the insert) [24]. In the composite ZnO(MA)/CdTe, a shift to superior energy is seen in the absorbance maxima because of contact between CdTe QDs with ZnO, yielding a band gap

value of 2.89 eV. Furthermore, the spectrum displayed a weak peak that appeared approximately at 500 nm, which is the characteristic surface plasma absorption corresponding to the CdTe nanoparticles in the sample. The results show that the ZnO(MA)/CdTe gives a broadened light absorption profile in the UV and visible scale, indicating that the composite ZnO(MA)/CdTe could allow more visible light absorption, therefore increasing its photocatalytic comportment [25,26].

### 2.3. Photocatalytic activity

The photocatalytic properties were determined by analyzing the degradation of CR as a pollutant under simulated sunlight irradiation. Fig. 2c shows the degradation of the dye for the ZnO (MA) / CdTe compounds with molar ratios of 1: 0.005, 1: 0.01, 1: 0.02 and 1: 0.03 and comparing them with CdTe and ZnO (MA) separately. The congo red dye sample does not show photocatalytic activity under irradiation and, the CdTe QDs and ZnO(MA) composite showed a lower photocatalytic behavior compared to the ZnO(MA)/CdTe composites. The photocatalytic activity of the ZnO(MA)/CdTe (1:0.02) compound did not show a substantial alteration with the performance of the ZnO(MA)/CdTe (1:0.03); this was probably because excessive CdTe QDs produced a light "shielding effect", which could affect the ZnO(MA) absorbed visible light, as observed in Fig. 2.c [15]. Therefore, the optimal ratio for the ZnO(MA)/CdTe (1:0.02) was selected. Certainly, as observed in Fig. 2c, the photocatalytic of ZnO(MA)/CdTe (1:0.02) in 120 min of irradiation was about 100%, which is considerably superior than that of ZnO(MA) of 50%, whereas only 4% degradation was observed not including the catalyst. Fig. 2d shows the variations in the UV–visible absorption spectra of CR at distinct times. CR has a typical absorption band at a wavelength of 497 nm. As the reaction progresses, the characteristic peaks slowly decrease as the reaction is irradiated. The insert
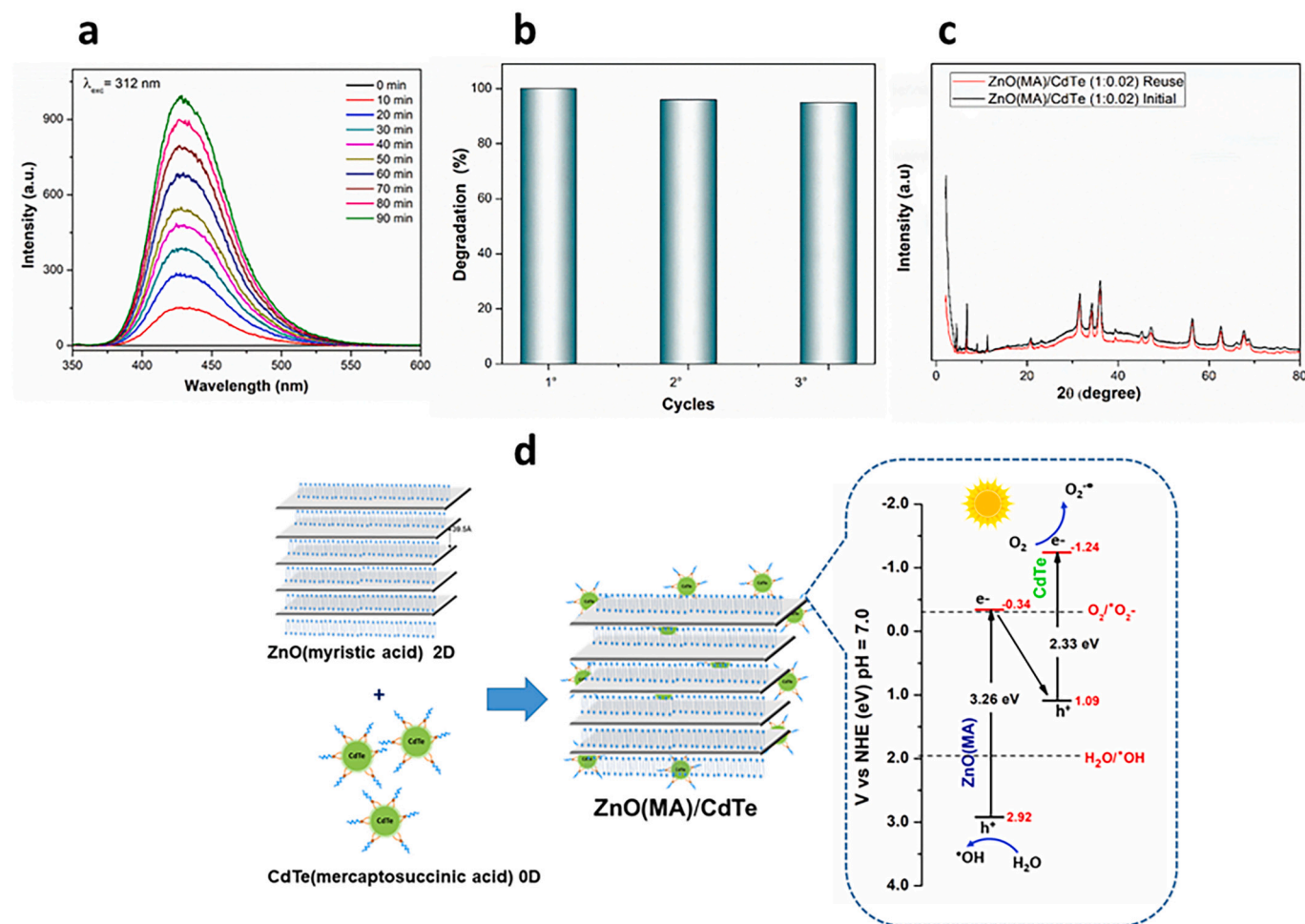
**Fig. 3.** (a) PL of ZnO(MA)/CdTe (1:0.02) in a solution of TA, (b) The recycling experiments for CR degradation of ZnO(MA)/CdTe (1:0.02) (c) XRD patterns of samples before and after reuse in photocatalytic degradation and (d) The proposed construction and photocatalytic reaction mechanism of the heterojunction ZnO (MA)/CdTe.

displays the color change of the CR solution in the time. To understand well the photocatalytic efficiency of the samples, they were investigated by pseudo first-order model, with $\ln(C_0/C) = kt$, where $k$ is the kinetic constant and $t$ is the irradiation time. Fig. 2e illustrates the linear fitting equation of the kinetics model. According to the correlation coefficients, the ZnO(MA)/CdTe (1:0.02) composite possessed the highest reaction rate, and the apparent rate constant ($k_{app}$, min$^{-1}$) is about 3 times faster than that of ZnO(MA) and 11 times faster than that of ZnO pristine. These results suggest that a coupling of 0D/2D shows excellent photocatalytic performance, which is assigned to the QDs that can act as electron traps to aid the separation of photoinduced electron-holes and ZnO (MA) layered with high surface exposure, with plus active sites accessible to expand matching with the surfaces of the CdTe in the photocatalytic activity [27]. Moreover, the existence of a hydrophobic organic moiety in ZnO(MA) promotes appreciably to the improved photocatalytic behavior, as observed in the aforementioned photocatalytic studies of hybrids of TiO$_2$ and ZnO [16, 37].

### 2.4. Proposed degradation mechanism

To additional investigate the probable mechanistic effects, we performed experiments using radical scavengers aiming to detect the species involved in photodegradation. Ammonium oxalate (AO) as the h$^+$ scavenger, benzoquinone (BQ) as the super oxide anion (O$_2^{\bullet-}$) scavenger and isopropyl alcohol (IPA) as the hydroxyl radicals ($^{\bullet}$OH) scavenger. As shown in Fig. 2f, the photodegradation activities are

appreciably inhibited when BQ and IPA are introduced, which indicates the following order h$+ <$ O$_2^{\bullet-} < {}^{\bullet}$OH for the active species participating in the photocatalytic degradation of the dye.

The hypothesis that $^{\bullet}$OH is equally an active species in the degradation was tested with terephthalic acid (TA) by the PL studies. We evaluated the rates of $^{\bullet}$OH formation in aqueous solution under irradiation. TA can react with the $^{\bullet}$OH radical to generate highly fluorescent 2-hydroxyterephthalic acid (TAOH). The peak intensity is proportional to the amount of produced $^{\bullet}$OH radicals. In Fig. 3a, the production rate of radical $^{\bullet}$OH can be identified, showing that the surface of the sample facilitates the production of ·OH radicals as photocatalytic intermediates to increase the photocatalytic activity in the degradation of the dye [28].

The electronic band alignment between CdTe and ZnO(MA) is done to recognize the charge transfer process and, thus, the probable mechanisms. The band gap values (Eg) of CdTe (2.33 eV) was estimated using the Tauc approach, cyclic voltammetry, and the UV–vis absorption spectra [29]. The band gap of ZnO(MA) (3.26 eV) was estimated from measured DRS using the Tauc plot. The conduction band (E$_{CB}$) and valence band (E$_{VB}$) of a semiconductor can be calculated by the equation: $E_{VB} = \chi - E^e + E_g/2$; $E_{CB} = E_{VB} - E_g$ [30]. In the Fig. 3d shows the band edge positions and band gaps.

Under simulated solar light irradiation, both ZnO(MA) and CdTe will be excited and generate photoinduced electrons and holes [31], the electrons on the CB of ZnO(MA) can move rapidly to recombine and eliminate with holes on the VB of CdTe at the interface due to the presence of the strong electrostatic attraction. The VB potential value of
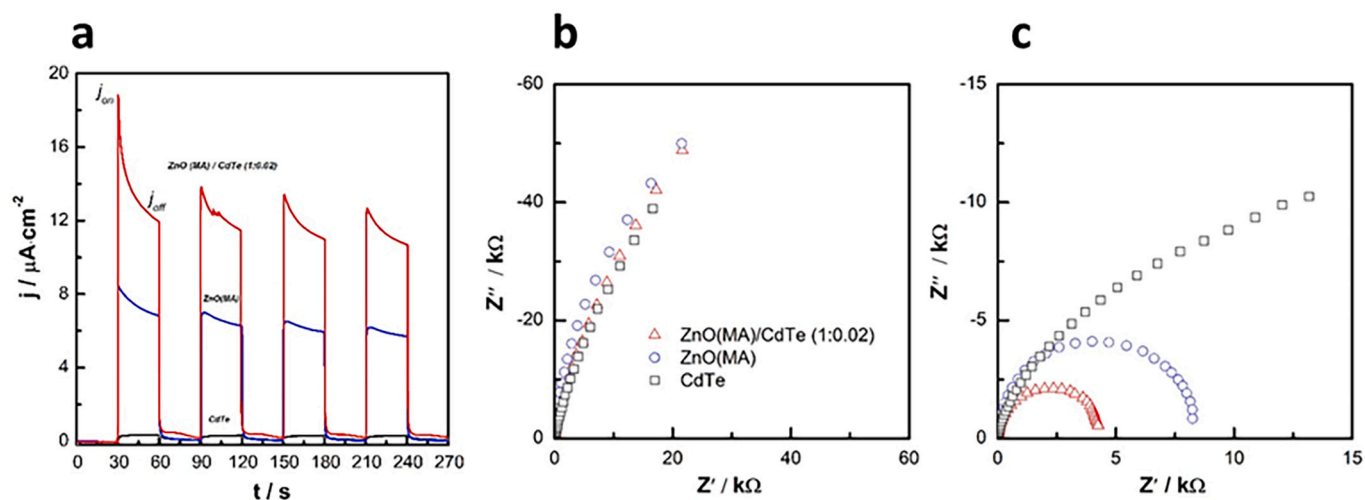
**Fig. 4.** (a) Photocurrent transients for electrodes (—) CdTe, (—)ZnO(MA), (—) ZnO(MA)/CdTe (1:0.02), (b) EIS and (c) PEIS spectra for electrodes (□) CdTe, (○) ZnO (MA), (Δ) ZnO(MA)/CdTe (1:0.02).

ZnO(MA) (2.92 V) is more active than $^{\bullet}OH/H_2O$ (1.99 eV vs NHE, pH = 7) and the CB potential of CdTe (− 1.24 V) is more passive than $O_2/O_2^{-\bullet}$ (−0.33 eV vs NHE, pH = 7). The charge separation and transfer of 0D/2D heterojunction follows the Z-scheme heterojunction, leaving photo-induced electrons and photoinduced holes with stronger redox capacities on the CB of CdTe and CV of ZnO(MA) respectively, favoring the formation of $O_2^{-\bullet}$ and $^{\bullet}OH$ radicals, leading to more efficient pollutant degradation.

The photocatalytic efficiency remained constant until the third cycle above 96% for 120 min, as shown in Fig. 3b. Furthermore, we have observed, by XRD, the stability of the sample after recycling in Fig. 3c, indicating the effective reuse of the sample without significant loss in the degradation efficiency.

*2.5. Electrochemical measurement*

The photoelectrochemical properties of the CdTe, ZnO(MA), and ZnO(MA)/CdTe (1:0.02) samples were analyzed. Fig. 4a shows the photocurrent response under the light on and light off cycles [32]. It is observed that The ZnO (MA)/CdTe (1: 0.02) electrode shows a higher photocurrent under illumination, than the CdTe and ZnO (MA) electrodes separately. These results are correlated with those obtained in the photocatalytic tests, demonstrating that the combined semiconductors lead to greater efficiency of charge separation and carrier availability due to the built-in electric field of heterojunction [33]. Electrochemical impedance spectroscopy (EIS) and photoelectrochemical impedance spectroscopy (PEIS) measurements were performed. Fig. 4b–c shows the Nyquist diagrams for the CdTe, ZnO (MA), and ZnO (MA) / CdTe (1: 0.02) samples. EIS measurements show an abrupt rise without defining semicircles throughout the sweep frequency spectrum due to absence charge carriers in the dark [34]. On the other hand, the Nyquist diagrams for the PEIS measurements show a pronounced decrease in the Z′ and Z′ values, accompanied by the definition of at least one semicircle associated with charge transfer at semiconductor/electrode interface [35]. The decrease in diameter of the semicircles in the Nyquist plots (CdTe <ZnO (MA) < ZnO (MA) / CdTe (1: 0.02)) is associated with an increase in the efficiency of the charge separation of the photogenerated e−/h + pairs and therefore an increase in interfacial electron transfer [36].

## 3. Conclusions

In summary, we have effectively prepared and characterized CdTe/ZnO(MA) heterostructure photocatalysts. The results indicated that a coupling of 0D/2D showed excellent photocatalytic performance, attributed to QDs that promote electron-hole separation and ZnO(MA) layered with high surface exposure, with plus active sites accessible to improve matching with the CdTe quantum dots in the photocatalytic activity. The synergy between the semiconductors generated the charge transfer and exhibited an improved solar light absorption, attributed to a Z-scheme mechanism demonstrating the clear contribution of CdTe and the ZnO(MA) in the photocatalytic degradation of Congo Red. The photocatalytic efficiency remained constant until the third cycle.

## Declaration of Competing Interest

The authors declare that they have no known competing financial interests or personal relationships that could have appeared to influence the work reported in this paper.

## Appendix A. Supplementary data

Supplementary data to this article can be found online at https://doi.org/10.1016/j.catcom.2021.106352.

## References

[1] J. Luo, S. Zhang, M. Sun, L. Yang, S. Luo, J.C. Crittenden, A critical review on energy conversion and environmental remediation of Photocatalysts with remodeling crystal lattice, surface, and Interface, ACS Nano 13 (2019) 9811–9840, https://doi.org/10.1021/acsnano.9b03649.

[2] S. Bera, D. Il Won, S.B. Rawal, H.J. Kang, W.I. Lee, Design of visible-light photocatalysts by coupling of inorganic semiconductors, Catal. Today 335 (2019) 3–19, https://doi.org/10.1016/j.cattod.2018.11.001.

[3] J. Sen Chang, J. Strunk, M.N. Chong, P.E. Poh, J.D. Ocon, Multi-dimensional zinc oxide (ZnO) nanoarchitectures as efficient photocatalysts: what is the fundamental factor that determines photoactivity in ZnO? J. Hazard. Mater. 381 (2020) 120958, https://doi.org/10.1016/j.jhazmat.2019.120958.

[4] R. Gang, L. Xu, Y. Xia, J. Cai, L. Zhang, S. Wang, R. Li, Fabrication of MoS2 QDs/ZnO nanosheet 0D/2D heterojunction photocatalysts for organic dyes and gaseous heavy metal removal, J. Colloid Interface Sci. 579 (2020) 853–861, https://doi.org/10.1016/j.jcis.2020.06.116.

[5] S. Manzeli, D. Ovchinnikov, D. Pasquier, O.V. Yazyev, A. Kis, 2D transition metal dichalcogenides, Nat. Rev. Mater. 2 (2017) 17033, https://doi.org/10.1038/natrevmats.2017.33.

[6] V. Reddy, R. Koutavarapu, K.R. Reddy, N. Shetti, T Aminabhavi, J Shim, Z-scheme binary 1D ZnWO4 nanorods decorated 2D NiFe2O4 nanoplates as photocatalysts for high-efficiency photocatalytic degradation of toxic organic pollutants from wastewater, J. Environ. Manag 268 (2020) 11677–11719, https://doi.org/10.1016/j.jenvman.2020.110677.

[7] J. Guo, P. Li, Z. Yang, A novel Z-scheme g- C3N4/LaCoO3 heterojunction with enhanced photocatalytic activity in degradation of tetracycline hydrochloride, Catal. Commun. 122 (2019) 63–67, https://doi.org/10.1016/j.catcom.2019.01.022.

[8] J. Low, C. Jiang, B. Cheng, S. Wageh, A.A. Al-Ghamdi, J. Yu, A review of direct Z-scheme photocatalysts, Small Methods. 1 (2017) 1700080, https://doi.org/10.1002/smtd.201700080.

[9] H. Li, W. Tu, Y. Zhou, Z. Zou, Z-scheme photocatalytic systems for promoting photocatalytic performance: recent progress and future challenges, Adv. Sci. 3 (2016) 1500389, https://doi.org/10.1002/advs.201500389.

[10] X. Yang, D. Wang, Photocatalysis: from fundamental principles to materials and applications, ACS Appl. Energy Mater. 1 (2018) 6657–6693, https://doi.org/10.1021/acsaem.8b01345.

[11] C. Eley, T. Li, F. Liao, S.M. Fairclough, J.M. Smith, G. Smith, S.C.E. Tsang, Nanojunction-mediated photocatalytic enhancement in heterostructured CdS/ZnO, CdSe/ZnO, and CdTe/ZnO nanocrystals, Angew. Chem. Int. Ed. 53 (2014) 7838–7842, https://doi.org/10.1002/anie.201404481.

[12] P. Sun, H. Zhang, C. Liu, J. Fang, M. Wang, J. Chen, J. Zhang, C. Mao, S. Xu, Preparation and characterization of Fe3O4/CdTe magnetic/fluorescent nanocomposites and their applications in immuno-labeling and fluorescent imaging of cancer cells, Langmuir. 26 (2010) 1278–1284, https://doi.org/10.1021/la9024553.

[13] R. Kaur, A. Rana, R.K. Singh, V.A. Chhabra, K.H. Kim, A. Deep, Efficient photocatalytic and photovoltaic applications with nanocomposites between CdTe QDs and an NTU-9 MOF, RSC Adv. 7 (2017) 29015–29024, https://doi.org/10.1039/c7ra04125j.

[14] X. Chen, X. Chen, X. Chen, X. Shen, X. Shen, S. Shen, M.O. Reese, S. Hu, S. Hu, Stable CdTe photoanodes with energetics matching those of a coating intermediate band, ACS Energy Lett. 5 (2020) 1865–1871, https://doi.org/10.1021/acsenergylett.0c00603.

[15] P. Yang, C. Chen, D. Wang, H. Ma, Y. Du, D. Cai, X. Zhang, Z. Wu, Kinetics, reaction pathways, and mechanism investigation for improved environmental remediation by 0D/3D CdTe/Bi2WO6 Z-scheme catalyst, Appl. Catal. B Environ. 285 (2021) 119877, https://doi.org/10.1016/j.apcatb.2021.119877.

[16] Y. Gong, Y. Wu, Y. Xu, L. Li, C. Li, X. Liu, L. Niu, All-solid-state Z-scheme CdTe/TiO2 heterostructure photocatalysts with enhanced visible-light photocatalytic degradation of antibiotic waste water, Chem. Eng. J. 350 (2018) 257–267, https://doi.org/10.1016/j.cej.2018.05.186.

[17] Q. Fang, B. Li, Y.Y. Li, W.Q. Huang, W. Peng, X. Fan, G.F. Huang, 0D/2D Z-scheme heterojunctions of g-C3N4 quantum dots/ZnO nanosheets as a highly efficient visible-light photocatalyst, Adv. Powder Technol. 30 (2019) 1576–1583, https://doi.org/10.1016/j.apt.2019.05.004.

[18] Y. Fu, W. Liang, J. Guo, H. Tang, S. Liu, MoS 2 quantum dots decorated g-C 3 N 4 /Ag heterostructures for enhanced visible light photocatalytic activity, Appl. Surf. Sci. 430 (2018) 234–242, https://doi.org/10.1016/j.apsusc.2017.08.042.

[19] C. Baslak, M. Demirel Kars, M. Karaman, M. Kus, Y. Cengeloglu, M. Ersoz, Biocompatible multi-walled carbon nanotube-CdTe quantum dot-polymer hybrids for medical applications, J. Lumin. 160 (2015) 9–15, https://doi.org/10.1016/j.jlumin.2014.11.030.

[20] M. Liu, W. Yao, C. Li, Z. Wu, L. Li, Tuning emission and stokes shift of CdS quantum dots via copper and indium co-doping, RSC Adv. 5 (2015) 628–634, https://doi.org/10.1039/c4ra11349g.

[21] M. Segovia, K. Lemus, M. Moreno, M.A.S. Ana, G. González, B. Ballesteros, C. Sotomayor, E. Benavente, Zinc oxide/carboxylic acid lamellar structures, Mater. Res. Bull. 46 (2011) 2191–2195, https://doi.org/10.1016/j.materresbull.2011.06.040.

[22] K. He, N. Chen, C. Wang, L. Wei, J. Chen, Method for determining crystal grain size by X-ray diffraction, Cryst. Res. Technol. 53 (2018) 1–6, https://doi.org/10.1002/crat.201700157.

[23] V. Zeleňák, Z. Vargová, K. Györyová, Correlation of infrared spectra of zinc(II) carboxylates with their structures, Spectrochim. Acta - Part A Mol. Biomol. Spectrosc. 66 (2007) 262–272, https://doi.org/10.1016/j.saa.2006.02.050.

[24] A.B. Murphy, Band-gap determination from diffuse reflectance measurements of semiconductor films, and application to photoelectrochemical water-splitting, Sol. Energy Mater. Sol. Cells 91 (2007) 1326–1337, https://doi.org/10.1016/j.solmat.2007.05.005.

[25] J. Briscoe, D.E. Gallardo, S. Hatch, V. Lesnyak, N. Gaponik, S. Dunn, Enhanced quantum dot deposition on ZnO nanorods for photovoltaics through layer-by-layer processing, J. Mater. Chem. 21 (2011) 2517–2523, https://doi.org/10.1039/c0jm02279a.

[26] X. Cao, P. Chen, Y. Guo, Decoration of textured ZnO nanowires array with CdTe quantum dots: enhanced light-trapping effect and photogenerated charge separation, J. Phys. Chem. C 112 (2008) 20560–20566, https://doi.org/10.1021/jp806645c.

[27] Y. Liu, F. Chen, Q. Li, H. Bao, Synthesis of CdTe/carbon nanotube/ZnO flower-like micro-spheres and their photocatalytic activities in degradation of rohdamine B, Mater. Lett. 210 (2018) 23–25, https://doi.org/10.1016/j.matlet.2017.08.111.

[28] Y. Fu, Z. Li, Q. Liu, X. Yang, H. Tang, Construction of carbon nitride and MoS2 quantum dot 2D/0D hybrid photocatalyst: direct Z-scheme mechanism for improved photocatalytic activity, Cuihua Xuebao/Chinese J. Catal. 38 (2017) 2160–2170, https://doi.org/10.1016/S1872-2067(17)62911-5.

[29] D. Guzmán, M. Isaacs, T. Tsukuda, S. Yamazoe, R. Takahata, R. Schrebler, A. Burgos, I. Osorio-Román, F. Castillo, CdTe quantum dots modified electrodes ITO-(Polycation/QDs) for carbon dioxide reduction to methanol, Appl. Surf. Sci. 509 (2020) 145386, https://doi.org/10.1016/j.apsusc.2020.145386.

[30] X. Yong, M.A.A. Schoonen, The absolute energy positions of conduction and valence bands of selected semiconducting minerals, Am. Mineral. 85 (2000) 543–556, https://doi.org/10.2138/am-2000-0416.

[31] Z. Youssef, L. Colombeau, N. Yesmurzayeva, F. Baros, R. Vanderesse, T. Hamieh, J. Toufaily, C. Frochot, T. Roques-Carmes, Dye-sensitized nanoparticles for heterogeneous photocatalysis: cases studies with TiO2, ZnO, fullerene and graphene for water purification, Dyes Pigments 159 (2018) 49–71, https://doi.org/10.1016/j.dyepig.2018.06.002.

[32] L.M. Peter, Energetics and kinetics of light-driven oxygen evolution at semiconductor electrodes: the example of hematite, J. Solid State Electrochem. 550 (2013) 315–326, https://doi.org/10.1007/s10008-012-1957-3.

[33] S. Xu, J. Jiang, W. Ren, H. Wang, R. Zhang, Y. Xie, Y. Chen, Construction of ZnO/CdS three-dimensional hierarchical photoelectrode for improved photoelectrochemical performance, Renew. Energy 153 (2020) 241–248, https://doi.org/10.1016/j.renene.2020.02.001.

[34] S. Sadhasivam, N. Anbarasan, M. Mukilan, P. Manivel, K. Jeganathan, Bi2S3 anchored ZnS/ZnO nanorod arrays photoanode for enhanced visible light driven photo electrochemical properties, Int. J. Hydrog. Energy 45 (2020) 30080–30090, https://doi.org/10.1016/j.ijhydene.2020.08.026.

[35] R. Ma, R. Pathak, D. Zheng, Y. Zhang, J. Xing, J. Liu, Y. Jiang, M. Xiao, F. Wu, Preparation and photoelectrochemical properties of hierarchical heterostructure ZnO/CuO array, Appl. Phys. A Mater. Sci. Process. 127 (2021) 1–9, https://doi.org/10.1007/s00339-020-04242-6.

[36] S.S. Hossain, M. Tarek, T.D. Munusamy, K.M. Rezaul Karim, S.M. Roopan, S. M. Sarkar, C.K. Cheng, M.M. Rahman Khan, Facile synthesis of CuO/CdS heterostructure photocatalyst for the effective degradation of dye under visible light, Environ. Res. 188 (2020), https://doi.org/10.1016/j.envres.2020.109803.